

# Improving critical dimension accuracy and throughput by subfield scheduling in electron beam mask writing

Sergey Babin<sup>a)</sup>

*ABeam Technologies, Castro Valley, California 94546*

Andrew B. Kahng<sup>b)</sup>

*CSE Department, University of California at San Diego, La Jolla, California 92093*

*and ECE Department, University of California at San Diego, La Jolla, California 92093*

Ion I. Măndoiu<sup>c)</sup>

*CSE Department, University of Connecticut, Storrs, Connecticut*

Swamy Muddu<sup>d)</sup>

*ECE Department, University of California at San Diego, La Jolla, California 92093*

(Received 28 June 2005; accepted 10 October 2005; published 6 December 2005)

Resist heating in high-voltage, high-throughput electron beam (e-beam) mask write is a significant source of critical dimension (CD) distortion. Excessive heating on the reticle determines changes in resist sensitivity, which in turn cause significant CD variation. CD distortions on the reticle are replicated onto the wafer with increased magnitude as determined by the mask error enhancement factor (MEEF). As designs enter the sub-90 nm regime, CD variation has a significant impact on performance, performance variation, and product yield. Previous methods for reducing CD distortion include usage of lower e-beam current density, increased delays between electron flashes, and multipass writing. However, all of these methods lower mask writing throughput, which is increasingly becoming a limiting factor in semiconductor industry productivity. In this paper, we propose a novel method for minimizing CD distortion and maximizing mask writing throughput. By scheduling the writing of subfields, we perform simultaneous optimization of mask writing order and e-beam current density. We perform subfield scheduling by evaluating resist temperature of subfield orderings using a fast analytical temperature model. Simulation experiments show that the new subfield scheduling method can reduce the maximum resist temperature up to 12 °C over existing sequential writing methods with unchanged mask writing throughput. Alternatively, improved subfield scheduling can enable the use of higher beam current densities, leading to increased writing throughput without compromising CD control. © 2005 American Vacuum Society. [DOI: 10.1116/1.2132330]

## I. INTRODUCTION

In high-voltage electron beam lithography, most of the beam energy is released as heat and accumulates in the local area of writing. Resist heating has been identified as a main contributor to critical dimension (CD) distortion in high-voltage electron beam mask making.<sup>1-4</sup> In an attempt to minimize CD distortion caused by resist heating, recent works<sup>5-8</sup> have explored the optimization of such parameters as beam current density, flash size, number of passes, and subfield writing order. A common drawback of these single-parameter optimizations is that the decreases in resist temperature are obtained at the expense of increasing mask writing time and cost.

In this paper, we propose a new method for minimizing CD distortion caused by resist heating. Our method performs simultaneous optimization of beam current density and subfield writing order, resulting in decreased resist heating with

unchanged mask writing throughput. To reduce excessive resist heating, we schedule the writing of subfields such that successively written subfields are far from each other. To maintain mask writing throughput, we simultaneously increase beam current density so that the resulting reduction in dwell time compensates for the increased travel and settling time caused by nonsequential writing of subfields. Simulations carried out using the commercially available TEMPTATION temperature simulation tool<sup>9</sup> show that the new subfield scheduling method leads to significant reductions in resist temperature compared to previous methods. Lower resist temperatures enable the use of higher beam current densities. This can reduce total writing time and hence increase throughput while keeping CD distortion within acceptable limits.

The rest of the paper is organized as follows: In Sec. II, we describe a subfield scheduling scheme based on the well-spaced labelings of rectangular grids introduced by Lagarias,<sup>10</sup> and then give a new greedy local improvement subfield scheduling algorithm. The greedy local improvement method starts from a random subfield schedule, and then iteratively improves it by swapping pairs of subfields in

<sup>a)</sup>Electronic mail: sb@abeamtech.com

<sup>b)</sup>Electronic mail: abk@ucsd.edu

<sup>c)</sup>Electronic mail: ion@engr.uconn.edu

<sup>d)</sup>Electronic mail: smuddu@ucsd.edu

1	17	33	49	65	81	97	113	129	145	161	177	193	209	225	241
248	8	24	40	56	72	88	104	120	136	152	168	184	200	216	232
239	255	15	31	47	63	79	95	111	127	143	159	175	191	207	223
214	230	246	6	22	38	54	70	86	102	118	134	150	166	182	198
205	221	237	253	13	29	45	61	77	93	109	125	141	157	173	189
180	196	212	228	244	4	20	36	52	68	84	100	116	132	148	164
171	187	203	219	235	251	11	27	43	59	75	91	107	123	139	155
146	162	178	194	210	226	242	2	18	34	50	66	82	98	114	130
137	153	169	185	201	217	233	249	9	25	41	57	73	89	105	121
128	144	160	176	192	208	224	240	256	16	32	48	64	80	96	112
103	119	135	151	167	183	199	215	231	247	7	23	39	55	71	87
94	110	126	142	158	174	190	206	222	238	254	14	30	46	62	78
69	85	101	117	133	149	165	181	197	213	229	245	5	21	37	53
60	76	92	108	124	140	156	172	188	204	220	236	252	12	28	44
35	51	67	83	99	115	131	147	163	179	195	211	227	243	3	19
26	42	58	74	90	106	122	138	154	170	186	202	218	234	250	10

FIG. 1. Subfield writing sequence for 16×16 Lagarias scheduling.

the schedule based on the effect on maximum and average resist temperature. The analytic approximation used for fast computation of resist temperature during the local improvement steps is described in Sec. III. In Sec. IV, we present the setup of our simulation experiments comparing the new greedy scheduling with previously proposed scheduling methods. Finally, in Sec. V we present the results and conclusions.

## II. SUBFIELD SCHEDULING ALGORITHMS

One of the most effective techniques for mitigating CD distortion caused by resist heating is to avoid sequential writing of features that are close to each other.<sup>5</sup> When performed at fracture granularity, non-sequential writing leads to unacceptable increases in total mask writing time due to the significant beam repositioning and settling time overheads. On the other hand, nonsequential writing of *subfields* incurs much smaller overheads relative to the total mask writing time. Therefore, we concentrate on techniques for improved nonsequential subfield scheduling.

In this section, we first review a subfield scheduling method due to Lagarias<sup>5,10</sup> and then give a new greedy local improvement subfield scheduling algorithm. The Lagarias schedule is based on pure geometric considerations (attempting to maximize the minimum Manhattan distance between

137	131	44	171	130	35	256	124	127	83	149	12	126	195	242	138
14	244	246	170	132	231	77	214	104	207	107	40	163	26	84	229
5	10	70	36	199	56	112	224	220	230	3	205	174	31	45	247
48	18	219	129	59	216	19	147	33	227	122	52	64	102	254	218
118	71	11	200	49	148	140	68	32	146	46	206	198	213	97	164
186	187	156	73	179	6	136	17	42	160	240	1	234	67	177	61
99	90	23	226	53	94	155	217	141	9	135	4	192	75	108	211
43	39	72	204	248	7	212	91	100	54	62	183	167	63	145	223
115	29	66	20	173	188	125	117	197	222	110	25	34	92	235	41
139	89	233	243	252	255	28	185	251	151	55	27	215	22	182	237
194	121	158	103	86	180	95	58	47	16	13	101	81	57	178	60
193	133	79	88	245	98	175	37	253	24	69	74	114	161	80	93
176	172	51	78	105	157	196	113	241	96	191	109	225	144	128	111
166	152	228	15	116	208	154	169	21	168	250	238	232	201	203	153
209	120	30	236	76	239	106	65	50	82	162	123	249	2	134	221
159	8	85	142	143	181	119	202	87	150	165	189	184	38	210	190

FIG. 2. Subfield writing sequence for 16×16 random schedule.

1	248	239	214	205	180	171	146	137	128	103	94	69	60	35	26
17	8	255	230	221	196	187	238	153	252	119	110	85	76	51	42
33	24	15	246	237	210	203	178	169	160	135	126	244	92	67	58
49	40	31	6	101	228	219	194	185	176	151	142	117	108	83	74
65	56	47	22	13	253	183	212	201	192	167	158	133	124	99	90
81	240	63	38	29	4	235	226	55	208	251	174	149	140	115	106
97	88	79	54	45	20	11	242	34	224	199	190	256	156	131	122
113	104	95	70	61	36	254	2	233	72	215	206	181	172	147	138
129	120	111	86	77	52	43	18	165	9	231	89	197	188	163	154
145	136	127	102	93	68	59	249	25	16	247	162	213	204	179	170
161	152	143	118	109	84	75	50	41	32	7	27	229	220	195	186
177	168	159	134	125	100	91	66	57	48	23	14	245	236	211	202
193	184	175	150	141	116	107	82	73	64	39	30	5	144	227	218
209	200	191	166	157	132	123	98	222	80	217	46	21	12	243	234
225	216	207	182	173	148	139	114	105	96	71	62	37	28	3	250
241	232	223	198	189	164	155	130	121	112	87	78	53	44	19	10

FIG. 3. Subfield writing sequence for 16×16 Greedy scheduling.

consecutively written subfields), whereas the greedy algorithm iteratively improves an initial random schedule by computing temperature of subfields using Green's function approximation.

## A. Lagarias scheduling

Motivated by applications to error-correction in two-dimensional memory arrays, Lagarias<sup>10</sup> introduced a class of "well-spaced labeling schemes" for rectangular grids which guarantees that the minimum Manhattan distance between grid nodes with consecutive labels is at most one less than the maximum possible. TEMPTATION simulations results show that Lagarias subfield scheduling can lead to significant reductions in maximum resist temperature compared to the sequential subfield scheduling currently used by electron beam mask writers.<sup>5</sup> However, these results were obtained using constant beam current density, which implies decreased throughput for the Lagarias scheduling due to the beam repositioning and settling overheads introduced by nonsequential writing of subfields. An interesting open question<sup>5</sup> is whether or not Lagarias scheduling leads to reductions in resist temperature in a normalized throughput setting, i.e., after increasing beam current density such that the resulting reduction in dwell time compensates for the increased travel and settling time in the Lagarias schedule. Simulation results reported in Sec. IV answer this question in the affirmative.

TABLE I. Mask and e-beam writer parameters.

Plate type	ZEP7000 resist on chrome and glass
Dimensions of main deflection field	1.024 mm × 1.024 mm
Dimensions of deflection subfield	64 μm × 64 μm
No. subfields	256
Flash size	2 μm × 2 μm
No flashes per subfield	512
Flash exposure time	1 μs (approx.)
Accelerating voltage	50 kV
Resist sensitivity	20 μC/cm <sup>2</sup>

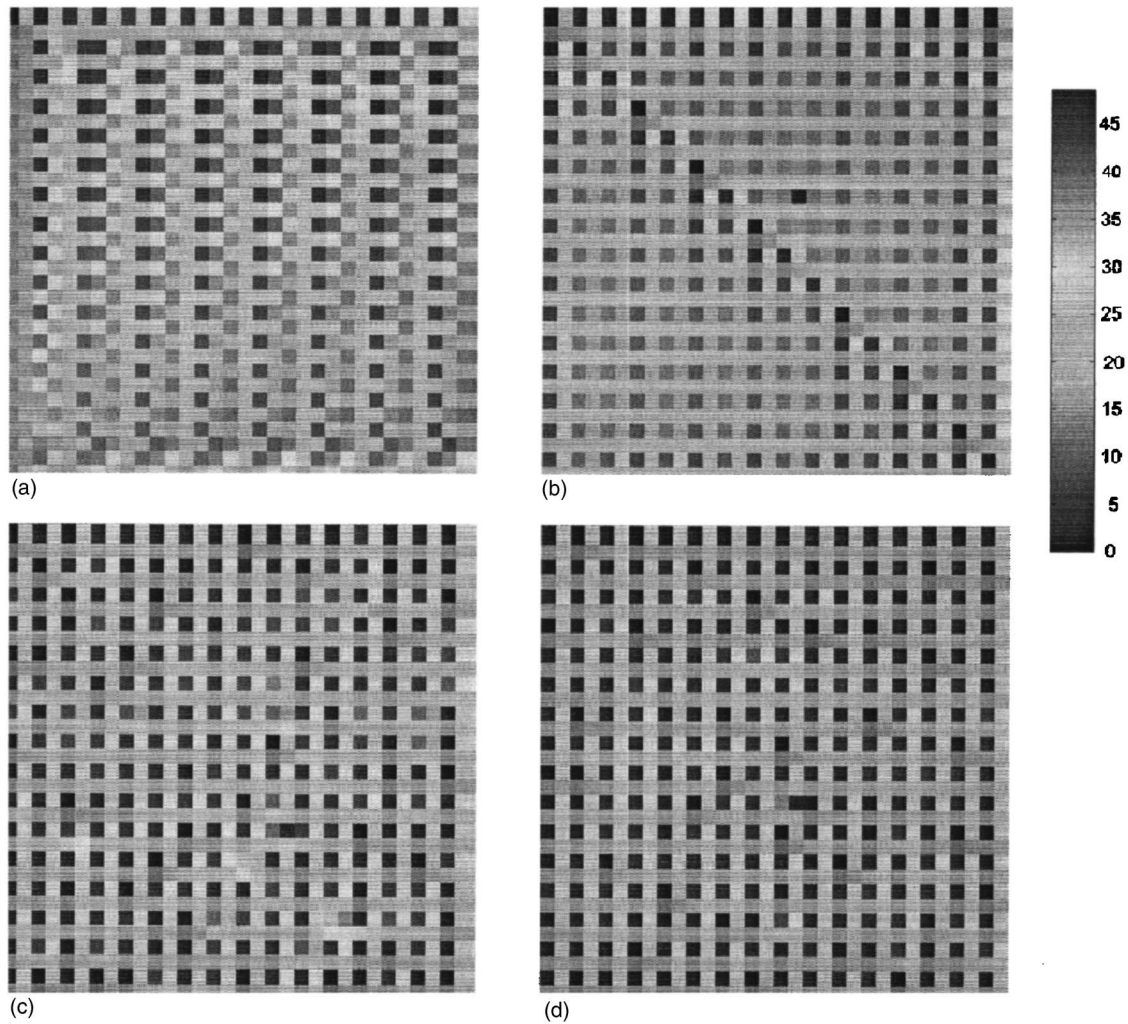


FIG. 4. Thermal profile of  $16 \times 16$  subfields for four writing schedules: (a) sequential, (b) Lagarias, (c) random, and (d) greedy. The color code shown is used for all writing schedules.

## B. Greedy local improvement algorithm

The main drawback of the Lagarias schedule is its exclusive reliance on geometric considerations. In particular, the schedule is insensitive to travel times between subfields. In this section, we give a greedy algorithm for finding subfield schedules that minimize the temperature experienced by resist. The algorithm is based on the local improvement paradigm, and relies on fast computation of subfield temperatures. An important feature of the model is that it can take into account travel times between subfields, which usually form a significant fraction of total writing time.

The greedy algorithm starts with a random subfield order, and then iteratively improves the order by swapping pairs of subfields. The algorithm evaluates available swaps using a cost function equal to  $\alpha T_{\max} + (1 - \alpha) T_{\text{average}}$ , where  $T_{\max}$  and  $T_{\text{average}}$  are the maximum, respectively, average subfield temperatures for the given order and  $\alpha$  is a parameter between 0 and 1 ( $\alpha$  is set to 0.5 in our experiments). In each iteration, the algorithm evaluates the cost function for schedules obtained from the current schedule by swapping single pairs of subfields. The swap that gives the largest decrease in the cost

function is then applied to the schedule, and the process is repeated until no further decreases in cost function are possible. Evaluating all possible pairs of subfields in each iteration would require  $O(n^2)$  cost function evaluations per iteration. Our implementation reduces the number of cost function evaluations per update to  $O(n)$  by considering only swaps of subfield pairs  $(i, j)$  in which  $i$  is a subfield with maximum temperature.

**Input:** Number of subfields  $n$ , mask writer parameters (voltage, current density, travel times, etc.)

**Output:** Subfield order  $\pi$ :

- (1) Generate initial subfield order  $\pi$  uniformly at random;
- (2) Repeat forever:

For all pairs  $(i, j)$  of subfields, compute cost of  $\pi$  with  $i$  and  $j$  swapped,

If there exists at least one cost improving swap, then modify  $\pi$  by applying a swap with highest cost gain,

Else, exit repeat;

- (3) Return subfield order  $\pi$ .

The key part of the greedy algorithm is the evaluation of the cost function. To compute the cost function, we must

evaluate the maximum and average temperature of a given subfield ordering. Evaluation of temperature evolution due to e-beam heating is well-studied in the literature.<sup>11,12</sup> Most of the approaches in the literature solve the classic thermodynamic equation with boundary conditions using finite difference method or Green's function approach. However, these approaches are too computationally intensive to be used for cost computation during the greedy algorithm. We propose an analytic approximation for the integral of Green's function to speed up temperature computation.

### III. TEMPERATURE COMPUTATION USING GREEN'S FUNCTION

In this section, we describe an efficient method for evaluating the cost function  $\alpha T_{\max} + (1 - \alpha) T_{\text{average}}$  for a fixed subfield schedule. To evaluate the rise in resist temperature, we first analyze the thermodynamic phenomenon after the occurrence of the e-beam flash. We then present Green's function solution of heat transfer due to single and multiple flashes. To reduce the complexity of computation, we give an analytic approximation and closed-form expressions for computing subfield resist temperatures.

Resist temperature at time  $t$  and location  $(x, y, z)$  depends on: (1) Distances from locations of e-beam flashes occurring prior to time  $t$ ; (2) Intensity of e-beam flashes (function of the e-beam parameters); and (3) Initial temperature at  $(x, y, z)$ . Occurrence of an e-beam flash at any point  $P(x', y', z')$  causes temperature at any location  $Q(x, y, z)$  to rise by an amount that is inversely proportional to the square

of the distance between  $P, Q$  and the initial temperature at  $Q$ . The temperature due to multiflash exposure is obtained by superimposing temperature responses due to individual exposures.

#### A. Single flash exposure

Temperature rise due to single flash exposure can be obtained from the heat diffusion equation

$$\frac{\partial T}{\partial t} = k \nabla^2 T + \frac{1}{\rho c^2} h, \quad (1)$$

where,  $T$  is the temperature rise in resist,  $k$  is thermal diffusivity of the resist,  $\rho$  is mass density, and  $c$  is specific heat of the resist. Here,  $h$  represents the energy distribution of the e-beam (heat source) and  $t$  represents the time duration. The temperature rise in the resist given by Eq. (1) can be solved using Green's function. The time-varying temperature distribution in three dimension  $(x, y, z)$  can be obtained by integrating Green's function,

$$\begin{aligned} T(x, y, z, t) = & \int_0^t dt' \int_{-a/2}^{a/2} dx' \int_{-b/2}^{b/2} dy' \int_{-d}^d \\ & \times G(x, y, z, t, x', y', z', t') \\ & \times h(x', y', z', t') dz'. \end{aligned} \quad (2)$$

Here,  $T(x, y, z, t)$  denotes the temperature at  $(x, y, z)$  in the resist at time  $t > t_e$  when an e-beam is shot at  $(x', y', z')$  during the time interval  $(0, t_e)$ , and  $G(x, y, z, t, x', y', z', t')$  is the Green's function given by

$$G(x, y, z, t, x', y', z', t') = \frac{1}{8(\sqrt{\pi k(t-t')})^3} \times \exp\left(-\frac{(x-x')^2 + (y-y')^2 + (z-z')^2}{4k(t-t')}\right). \quad (3)$$

In Eq. (2),  $h(x', y', z', t')$  represents the energy distribution of the e-beam centered at  $(x', y', z')$ , contained within the volume  $a \times b \times d$ , occurring at time instant  $t'$ , which is given by<sup>14</sup>

$$\begin{aligned} h(x', y', z', t) = & V \cdot Q \cdot \lambda(z/R_g) \cdot S(x'/a) \\ & \cdot S(y' \cdot b) \cdot S(t'/\theta)/(R_g \cdot \theta), \end{aligned} \quad (4)$$

where  $S$  is a unit square function in the interval  $0 \leq u \leq 1$ , and  $V, Q, R_g$  and  $\theta$  represent the acceleration voltage of the e-beam, resist sensitivity, Gruen range,<sup>13</sup> and exposure duration, respectively. The function  $\lambda$  represents the electron energy loss distribution perpendicular to the surface of resist. Equation (4) gives the amount of heat induced in the volume  $a \times b \times R_g$  in the resist over a period  $\theta$ . Electrons in the high energy e-beams impinged on the resist penetrate the surface and traverse diverse paths before coming to a stop. Gruen range indicates the average distance an electron travels inside the resist. (Accurate computation of the amount of heat dis-

sipated due to electron traversals can be obtained from Monte Carlo simulations. Modeling electron trajectories and computation of exact heat dissipation is well-studied in the literature, and hence not discussed here.) The maximum value of  $z$  is  $0.5 \mu\text{m}$  and that of  $R_g$  is  $10 \mu\text{m}$ .<sup>13</sup> The value of  $\lambda(z/R_g)$  approaches unity in this case. The value of  $S(\cdot)$  in the heat generation function also equals unity in the range of values considered. Substituting  $h$  in Eq. (2) and evaluating the integral, we get

$$\begin{aligned} T(x, y, z, t) = & \frac{VQ}{R_g \theta 32k} \int_0^{t_e} \left[ \operatorname{erf}\left(\frac{a/2+x}{\sqrt{p}}\right) + \operatorname{erf}\left(\frac{a/2-x}{\sqrt{p}}\right) \right] \\ & \times \left[ \operatorname{erf}\left(\frac{b/2+y}{\sqrt{p}}\right) + \operatorname{erf}\left(\frac{b/2-y}{\sqrt{p}}\right) \right] \\ & \times \left[ \operatorname{erf}\left(\frac{c}{\sqrt{p}}\right) \right] dt'. \end{aligned} \quad (5)$$

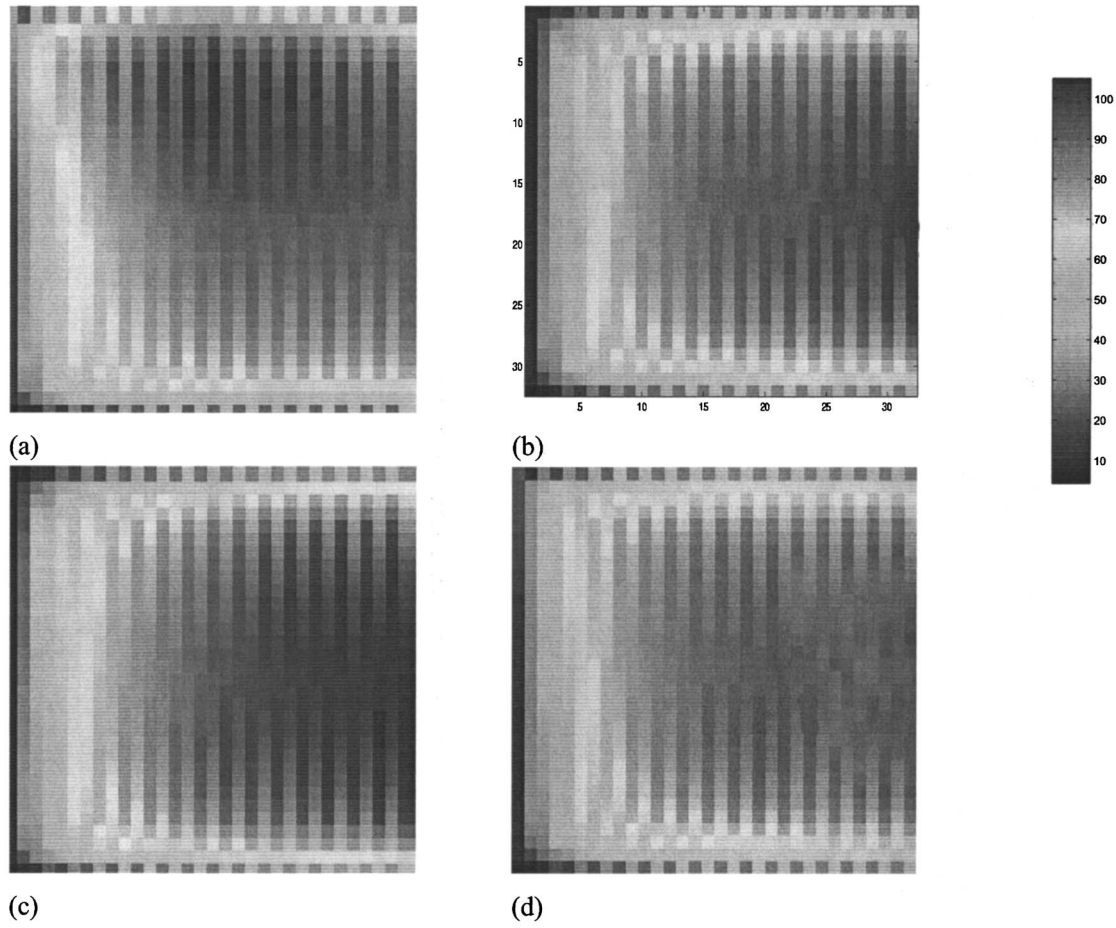


FIG. 5. Thermal profile of the critical subfield (the subfield with maximum temperature) for four writing schedules: (a) sequential, (b) Lagarias, (c) random, and (d) greedy. The color code shown is used for all writing schedules.

**B. Multiple flash exposure**

To compute the temperature profile of all the subfields during a complete flashing sequence, we must analyze the temperature evolution with multiple flashes. In a multiple flash scenario, the energy distribution function  $h$  is a sum of energy impulses separated in space and time. The temperature response to this train of impulses can be obtained by integrating  $h$  using Eq. (2). The heat generation function  $h$  over entire flashing duration can be represented as  $h = \sum_i h(x_i, y_i, z_i, t_i)$  where  $i \in \{1, \dots, n\}$  and  $h(x_i, y_i, z_i, t_i)$  are defined as follows:

$$h(x_i, y_i, z_i, t_i) = \begin{cases} 0 & \forall i \neq j \text{ where } i, j \in \{1, \dots, n\} \\ \frac{VQ}{R_g \theta} \lambda(z_i/R_g) \cdot S(x_i/a) \cdot S(y_i/b) \cdot S(t_i/\theta) & \text{otherwise.} \end{cases} \tag{6}$$

The variable  $i$  corresponds to the flashing point and  $j$  corresponds to the destination.

The temperature at any location  $(x, y, z)$  at time  $t$  within the entire flashing duration is the sum of temperature re-

sponses due to individual flashes. Computing resist temperature due to flashing individual fractures within each subfield leads to prohibitive running time. Hence, we compute subfield temperatures assuming e-beam footprint of the size of subfields. Subfield temperature is computed for the entire flashing duration with very fine granularity and is measured at the center of each subfield. For every flash, we compute temperature response of all subfields. These responses are summed up for all the flashes over entire flashing duration to obtain complete subfield temperature profile.

To reduce the complexity of temperature computation during evaluation of subfield orderings, we give an analytic approximation for Eq. (5). Based on the approximation, eight possible cases of various time-distance ranges were considered. The result of integration for each case is given below:

Case 1:  $\sqrt{t_{a1}}, \sqrt{t_{a2}}, \sqrt{t_{b1}}, \sqrt{t_{b2}}, \sqrt{t_c} < \sqrt{\pi}/2,$   
 Integrand =  $\frac{2}{3}(A_1 + A_2) \cdot (B_1 + B_2) \cdot C \cdot p^{-3/2}$

Case 2:  $\sqrt{t_{a1}} > \sqrt{\pi}/2, \sqrt{t_{a2}}, \sqrt{t_{b1}}, \sqrt{t_{b2}}, \sqrt{t_c} < \sqrt{\pi}/2,$   
 Integrand =  $(B_1 + B_2) \cdot C \cdot (\log p - (2A_2/\sqrt{p}))$

$$\text{Case 3: } \sqrt{t_{a1}}, \sqrt{t_{a2}} > \sqrt{\pi/2}, \sqrt{t_{b1}}, \sqrt{t_{b2}}, \sqrt{t_c} < \sqrt{\pi/2},$$

$$\text{Integrand} = 2(B_1 + B_2) \cdot C \cdot \log p$$

$$\text{Case 4: } \sqrt{t_{a1}}, \sqrt{t_{a2}}, \sqrt{t_{b1}} > \sqrt{\pi/2}, \sqrt{t_{b2}}, \sqrt{t_c} < \sqrt{\pi/2},$$

$$\text{Integrand} = 2C \cdot (p + B_2 \cdot \log p)$$

$$\text{Case 5: } \sqrt{t_{a1}}, \sqrt{t_{a2}}, \sqrt{t_{b1}}, \sqrt{t_{b2}} > \sqrt{\pi/2}, \sqrt{t_c} < \sqrt{\pi/2},$$

$$\text{Integrand} = 4C \cdot p$$

$$\text{Case 6: } \sqrt{t_{a1}}, \sqrt{t_{a2}}, \sqrt{t_{b1}}, \sqrt{t_{b2}}, \sqrt{t_c} > \sqrt{\pi/2}, \text{Integrand} = 4p^2$$

$$\text{Case 7: } \sqrt{t_{a1}}, \sqrt{t_{b1}} > \sqrt{\pi/2}, \sqrt{t_{a2}}, \sqrt{t_{b2}}, \sqrt{t_c} < \sqrt{\pi/2},$$

$$\text{Integrand} = C \cdot (p + (A_2 + B_2) \cdot \log p - (A_2 B_2 / p))$$

$$\text{Case 8: } \sqrt{t_{a1}}, \sqrt{t_{b1}}, \sqrt{t_c} > \sqrt{\pi/2}, \sqrt{t_{a2}}, \sqrt{t_{b2}} < \sqrt{\pi/2},$$

$$\text{Integrand} = (p^2/2) + (A_2 + B_2) \cdot p + A_2 \cdot B_2 \cdot \log p,$$

where  $A_1 = a/2 + x$ ,  $A_2 = a/2 - x$ ,  $B_1 = b/2 + y$ ,  $B_2 = b/2 - y$ ,  $C = c$ ,  $t_{a1} = A_1^2/p$ ,  $t_{a2} = A_2^2/p$ ,  $t_{b1} = B_1^2/p$ ,  $t_{b2} = B_2^2/p$ , and  $t_c = C^2/p$ .

#### IV. SIMULATION SETUP AND PARAMETERS

In this section, we describe the experimental setup for thermal simulations of different subfield writing schedules. We used the commercial TEMPTATION software<sup>9</sup> for simulating the thermal evolution of the resist during e-beam exposure of compared scheduling strategies. The TEMPTATION software has been subjected to extensive experimental verification showing that TEMPTATION predicted temperatures are in excellent agreement with measured temperatures.<sup>9</sup> We simulated four scheduling strategies:

- (1) **Sequential writing schedule:** In this schedule, conventionally used by e-beam writers, writing starts at a corner of the major field and proceeds in a sequential serpentine fashion.
- (2) **Lagarias writing schedule:** In this schedule, writing is performed according to the order specified by the analytical formulas given in Ref. 10. The Lagarias order for  $16 \times 16$  subfields is given in Fig. 1.
- (3) **Random writing schedule:** We used the randomly generated order for  $16 \times 16$  subfields in Fig. 2.
- (4) **Greedy writing schedule:** In this schedule, writing is performed based on the order computed by the greedy local improvement described in Sec. II B. The order is shown in Fig. 3.

We simulated a major field of size  $1.024 \text{ mm} \times 1.024 \text{ mm}$ , divided into  $16 \times 16$  subfields of size  $64 \mu\text{m} \times 64 \mu\text{m}$  each. For each subfield we simulated a chess board fracture pattern exposed in sequential-serpent order. Mask and e-beam parameters used in our TEMPTATION simulations are given in Table I. For each subfield scheduling, the simulation was performed in two phases. In the first simulation phase, each of the 256 subfields was exposed to four coarse flashes that delivered to the subfield the same dose as the detailed chess board fracture flashes. Furthermore, the

four doses were specified such that subfield writing time was identical to that required by detailed chess board fracture flashes. This coarse simulation captures the effect of subfield scheduling on the *average* subfield temperature before writing.

During first simulation phase, delays were introduced between subfield flashes to simulate the effect of travel and settling time between subfields. In our simulations we assumed a constant settling time of 25 ns and a travel time proportional to the maximum distance traveled in either the horizontal or vertical direction. More exactly, the settling time was computed using the formula  $25 \text{ ns} + 5 \text{ ns} \times \max\{\Delta x, \Delta y\}$ , where  $\Delta x$  and  $\Delta y$  are the horizontal and vertical travel distances, respectively. To maintain constant throughput among various subfield writing schedules, we increased the beam current density to reduce the dwell time by an amount equal to the overhead in travel and settling times. The resulting current density values were  $20.0 \text{ A/cm}^2$  for sequential,  $21.3 \text{ A/cm}^2$  for random,  $21.8 \text{ A/cm}^2$  for Lagarias, and  $21.5 \text{ A/cm}^2$  for the greedy subfield order.

As a result of first phase simulations we identified for each subfield ordering the subfield with the largest average temperature before writing, which we call ‘‘critical’’ subfield. Detailed fracture flashing was then simulated for each of the four critical subfields corresponding to each ordering.

#### V. RESULTS AND CONCLUSIONS

Figure 4 shows the temperature before writing for each of the  $16 \times 16$  subfields under the four considered writing schedules. The greedy, Lagarias and random schedules have a lower average subfield temperature compared to the sequential schedule. The maximum subfield temperature is lower for the greedy schedule than for the Lagarias and random.

Figure 5 shows the temperature before writing for the fractures in the critical subfields corresponding to the four simulated schedules. The results show that the worst fracture temperature before writing for the greedy order is reduced to  $92.87 \text{ }^\circ\text{C}$  compared to  $105.1 \text{ }^\circ\text{C}$  for sequential,  $104.6 \text{ }^\circ\text{C}$  for random, and  $97.15 \text{ }^\circ\text{C}$  for Lagarias order. The lower resist temperature enables the use of a higher beam current density. Depending on the particular parameters of the writer, this can reduce total writing time and hence increase throughput while keeping CD distortion within acceptable limits.

In this paper we have presented an exploratory approach for mitigating CD distortions caused due to resist heating during e-beam writing. Nonsequential writing of subfields within the main deflection field requires modifications to the e-beam writer hardware to position the e-beam accurately. The reductions in resist temperatures due to nonsequential writing provide a motivation for architectural changes to e-beam writers of the future.

<sup>1</sup>N. Kuwahara, H. Nakagawa, M. Kurihara, N. Hayashi, H. Sano, E. Murata, T. Takikawa, and S. Noguchi, Proc. SPIE **3784**, 115 (1999).

<sup>2</sup>S. Babin, J. Vac. Sci. Technol. B **15**, 2209 (1997).

<sup>3</sup>K. Nakajima and N. Aizaki, J. Vac. Sci. Technol. B **10**, 2784 (1992).

<sup>4</sup>H. Sakurai, T. Abe, M. Itoh, A. Kumagai, H. Anze, and I. Higashikawa,

- Proc. SPIE **3748**, 126 (1999).
- <sup>5</sup>S. Babin, A. B. Kahng, I. I. Mandoiu, and S. Muddu, Proc. SPIE **5130**, 719 (2003).
- <sup>6</sup>S. Babin and I. Y. Kuzmin, Proc. SPIE **4562**, 545 (2002); **16**, 3241 (1998).
- <sup>7</sup>L. H. Veneklasen, J. Vac. Sci. Technol. B **9**, 3063 (1991).
- <sup>8</sup>S. Babin, Microelectron. Eng. **53**, 341 (2000).
- <sup>9</sup>S. Babin and I. Y. Kuzmin, J. Vac. Sci. Technol. B **16**, 3241 (1998).
- <sup>10</sup>J. C. Lagarias, SIAM J. Discrete Math. **13**, 521 (2000).
- <sup>11</sup>I. Y. Kuzmin, Proc. SPIE **3676**, 536 (1999).
- <sup>12</sup>D. Chu, F. W. Pease, and K. Goodson, "Modeling Resist Heat in Mask Fabrication using a Multi-layer Green's Function Approach," SPIE'02 Manuscript, <http://www.stanford.edu/~dcchu>
- <sup>13</sup>K. A. Valiev, *The Physics of Submicron Lithography* (Plenum, New York, 1992), p. 9609.
- <sup>14</sup>T. Abe, K. Ohta, H. Wada, and T. Takigawa, J. Vac. Sci. Technol. B **6**, 853 (1988).